

Preparation and Characterization of Nano-Magnetic $Mn_{0.5}Zn_{0.5}Fe_2O_4$ System

N. M. Deraz* and A. Alarifi¹

Chemistry Department, College of Science, King Saud University, P.O. Box 2455, Riyadh 11451, Saudi Arabia.

*E-mail: nmderaz@yahoo.com

Received: 21 May 2012 / Accepted: 6 June 2012 / Published: 1 July 2012

X-ray diffraction (XRD), Scanning electron micrographs (SEM) and Energy dispersive X-ray (EDX) techniques were used to characterize $Mn_{0.5}Zn_{0.5}Fe_2O_4$ nano-particles synthesised by advanced combustion route. The magnetic properties of the as prepared sample were determined by using vibrating sample magnetometer (VSM). The preparation method investigated brought about formation of single spinel $Mn_{0.5}Zn_{0.5}Fe_2O_4$ phase. The values of saturation magnetization (85emu/g), the remnant magnetization (22 emu/g) and coercivity (58 Oe) of $Mn_{0.5}Zn_{0.5}Fe_2O_4$ particles were found to be high due to their elevated particle size. Our results indicate that the mixed ferrites with the composition of $Mn_{0.5}Zn_{0.5}Fe_2O_4$ have a high saturation magnetization comparing with simple ferrites with the composites' of $MnFe_2O_4$ and $ZnFe_2O_4$.

Keywords: XRD; SEM, EDX; M_s , $Mn_{0.5}Zn_{0.5}Fe_2O_4$.

1. INTRODUCTION

Spinel ferrites, with a generalized formula AB_2O_4 , have attracted considerable interest due to their remarkable properties such as optical, mechanical, thermal, and magnetic properties. There are different technological applications such as high density magnetic recording, biomedicine, targeted drug delivery, magnetic fluids, data storage, spin-tonics, solar cells, sensors, and catalysis [1–4]. The different properties of spinel structure are controlled by the cation distribution between the tetrahedral A-site and octahedral B-site. The cation distribution depends on the ionic radii of cations, preparation method, preparation conditions, chemical composition, sintering temperature, doping and substitution process [5-9].

Recently, processing of ferrites with high performance has great importance to meet the technological challenges. Thus the quality of ferrite powders has strong influence on the performance of final device. So, various chemical methods were developed to prepare nano-crystalline spinel

ferrites. These methods include wet chemical co-precipitation, microwave refluxing, sol-gel, hydrothermal, glass crystallization, salt melt technique and combustion route [5-14].

Zinc ferrite, ZnFe_2O_4 is a normal spinel structure, where Zn^{2+} preferably occupy the tetrahedral sites due to their affinity for sp^3 bonding with oxygen anions leaving all the ferric ions on the octahedral sites. The normal spinel structured ZnFe_2O_4 is paramagnetic at room temperature due to weak superexchange interaction which could be attributed to right angle in $\text{Fe}^{3+}\text{-O-Fe}^{3+}$ [14]. Furthermore, MnFe_2O_4 has partially inversed spinels structure consisting of, manganese and ferric ions occupying both tetrahedral (A) and octahedral (B) sites [15, 16].

Manganese–zinc (Mn–Zn) ferrites exhibit some unique properties such as enhanced coercivity, modified saturation magnetization, super paramagnetism, and metastable cation distributions [17]. Mn-Zn ferrites have many applications in heat transfer devices, drug delivery systems, and medical diagnostics especially in cancer treatment [18, 19]. Mn-Zn ferrites possess a spinel structure in which Mn^{2+} , Zn^{2+} , and Fe^{3+} cations are distributed among two interstitial tetrahedral and octahedral sites. So, the Mn-Zn ferrites have mixed spinel structure. In addition, the magnetic and electronic properties of these ferrites are dependent of their chemical composition, preparation method, grain size and distribution of cation between two interstitial sites [20, 21].

In the current study, focus was placed on development of a synthesis route for $\text{Mn}_{0.5}\text{Zn}_{0.5}\text{Fe}_2\text{O}_4$ nano-particles via glycine-assisted combustion method and examining the structural, morphological and magnetic properties.

2. EXPERIMENTAL

2.1. Materials

Nano- particles of $\text{Mn}_{0.5}\text{Zn}_{0.5}\text{Fe}_2\text{O}_4$ sample was prepared by mixing calculated proportions of manganese, zinc and iron nitrates with a mixture of glycine and ammonium nitrate. The mixed precursors were concentrated in a porcelain crucible on a hot plate at 350 °C for 10 minutes. The crystal water was gradually vaporized during heating and when a crucible temperature was reached, a great deal of foams produced and spark appeared at one corner which spread through the mass, yielding a brown voluminous and fluffy product in the container. In our experiment, the ratio of the H_4NNO_3 : $\text{H}_2\text{NCH}_2\text{COOH}$: $\text{Mn}(\text{NO}_3)_2 \cdot 4\text{H}_2\text{O}$: $\text{Zn}(\text{NO}_3)_2 \cdot 6\text{H}_2\text{O}$: $\text{Fe}(\text{NO}_3)_3 \cdot 9\text{H}_2\text{O}$ were 1: 4 : 0.5 : 0.5 : 2, respectively. The chemicals employed in the present work were of analytical grade supplied by Prolabo Company.

2.2. Techniques

An X-ray measurement of various mixed solids was carried out using a BRUKER D8 advance diffractometer (Germany).

The patterns were run with Cu K_α radiation at 40 kV and 40 mA with scanning speed in 2θ of 2 ° min^{-1} .

The crystallite size of $\text{Mn}_{0.5}\text{Zn}_{0.5}\text{Fe}_2\text{O}_4$ present in the investigated solids was based on X-ray diffraction line broadening and calculated by using Scherrer equation [22].

$$d = \frac{B\lambda}{\beta \cos \theta} \quad (1)$$

where d is the average crystallite size of the phase under investigation, B is the Scherrer constant (0.89), λ is the wave length of X-ray beam used, β is the full-width half maximum (FWHM) of diffraction and θ is the Bragg's angle.

Scanning electron micrographs (SEM) were recorded on SEM-JEOL JAX-840A electron micro-analyzer (Japan). The samples were dispersed in ethanol and then treated ultrasonically in order to disperse individual particles over a gold grid.

Energy dispersive X-ray (EDX) analysis was carried out on Hitachi S-800 electron microscope with an attached kevox Delta system. The parameters were as follows: accelerating voltage 10, 15 and 20 kV, accumulation time 100s, window width $8 \mu\text{m}$. The surface molar composition was determined by the Asa method, Zaf-correction, Gaussian approximation.

The magnetic properties of the investigated solids were measured at room temperature using a vibrating sample magnetometer (VSM; 9600-1 LDJ, USA) in a maximum applied field of 15 kOe. From the obtained hysteresis loops, the saturation magnetization (M_s), remanence magnetization (M_r) and coercivity (H_c) were determined.

3. RESULTS

3.1. XRD study

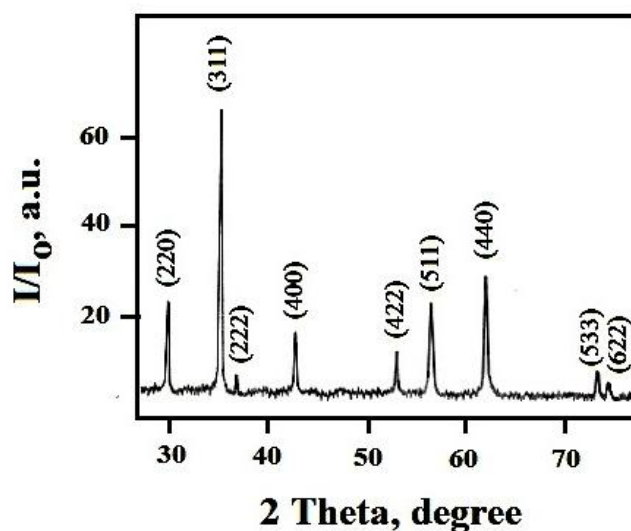


Figure 1. XRD pattern for $\text{Mn}_{0.5}\text{Zn}_{0.5}\text{Fe}_2\text{O}_4$ sample.

Fig. 1 showed XRD pattern for the as prepared sample which consisted entirely of nano-crystalline $\text{Mn}_{0.5}\text{Zn}_{0.5}\text{Fe}_2\text{O}_4$ phase with the $Fd3m$ space group depending upon JCPDS card No. 75-0034. The crystal planes of the spinel $\text{Mn}_{0.5}\text{Zn}_{0.5}\text{Fe}_2\text{O}_4$ phase are (220), (311), (222), (400), (422), (511), (440), (533) and (622), respectively. The average crystallite size of $\text{Mn}_{0.5}\text{Zn}_{0.5}\text{Fe}_2\text{O}_4$ phase was estimated to be about 67 nm. No additional peak of the second phase was observed in the XRD pattern, showing that the as prepared ferrite consisted of single spinel $\text{Mn}_{0.5}\text{Zn}_{0.5}\text{Fe}_2\text{O}_4$ phase. From the data of X-ray, various structural parameters such as the lattice constant (a), unit cell volume (V), X-ray density (D_x), the distance between the magnetic ions (L_A and L_B), ionic radii (r_A , r_B) and bond lengths ($A-O$ and $B-O$) on tetrahedral (A) sites and octahedral (B) sites of $\text{Mn}_{0.5}\text{Zn}_{0.5}\text{Fe}_2\text{O}_4$ crystallites were determined. The calculated values of a , L_A , L_B , r_A , r_B , $A-O$ and $B-O$ of Mn ferrite are 0.8482, 0.3673, 0.2999, 0.0560, 0.0728, 0.1910 and 0.2078 nm, respectively. Whereas, the value of V is 0.6102 nm^3 while the value of D_x is 5.13256 g/cm^3 .

3.2. SEM measurement

Fig. 2a-d shows SEM images for the as prepared $\text{Mn}_{0.5}\text{Zn}_{0.5}\text{Fe}_2\text{O}_4$ powders. We can see from this figure that the as synthesized powders are spongy and fragile. In addition, voids and pores are observed in the as prepared sample. These findings could be attributed to the release of large amounts of gases during combustion process due to the decomposition of both glycine and ammonium nitrate. However, using a mixture of glycine with ammonium nitrate led to formation of multigrain agglomerations with the fracture surfaces. By comparing this work with the different studies in the literatures, it was found that the $\text{Mn}_{0.5}\text{Zn}_{0.5}\text{Fe}_2\text{O}_4$ prepared by using a mixture of glycine and ammonium nitrate displays weak agglomeration.

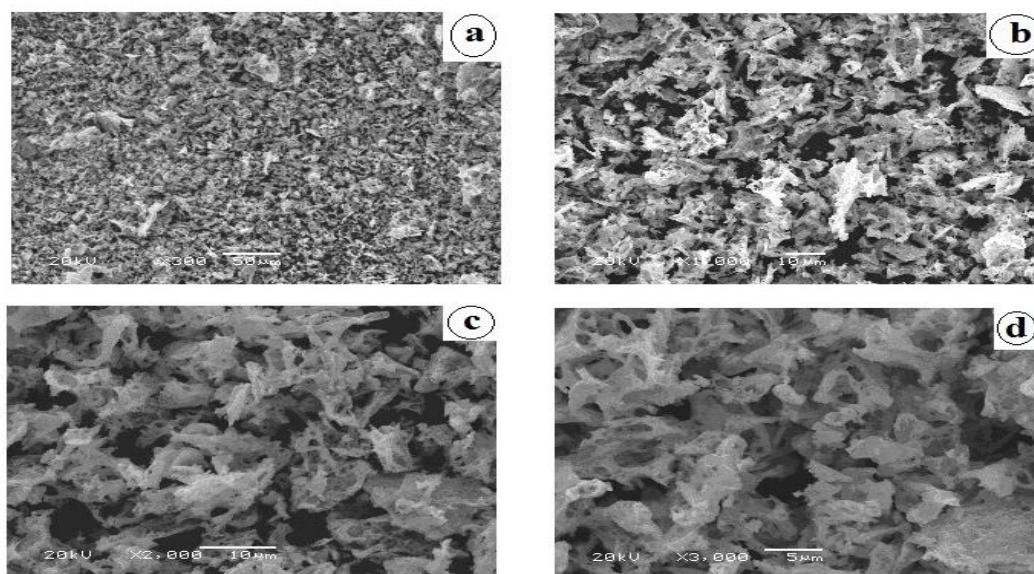


Figure 2. SEM images for $\text{Mn}_{0.5}\text{Zn}_{0.5}\text{Fe}_2\text{O}_4$ sample with different magnifications.

3.3. EDX analysis

Energy dispersive X-ray (EDX) analysis with different voltages and various areas on the surface of sample studied was carried out. Figs. 3 and 4 display EDX analysis with different voltages and various areas, respectively.

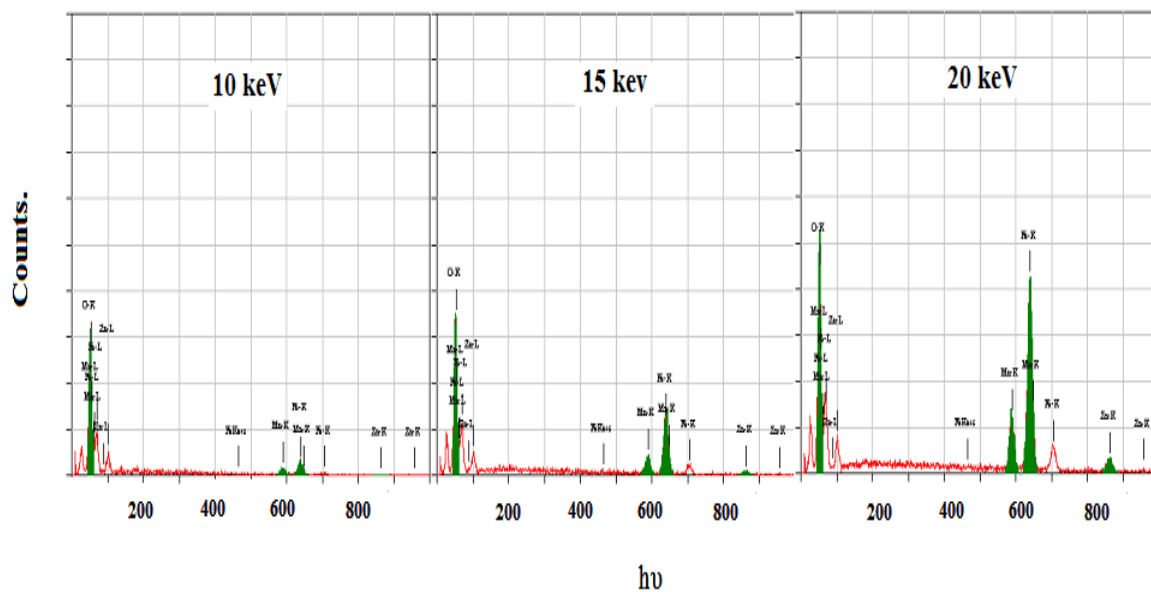


Figure 3. EDX pattern of $Mn_{0.5}Zn_{0.5}Fe_2O_4$ sample with different voltages.

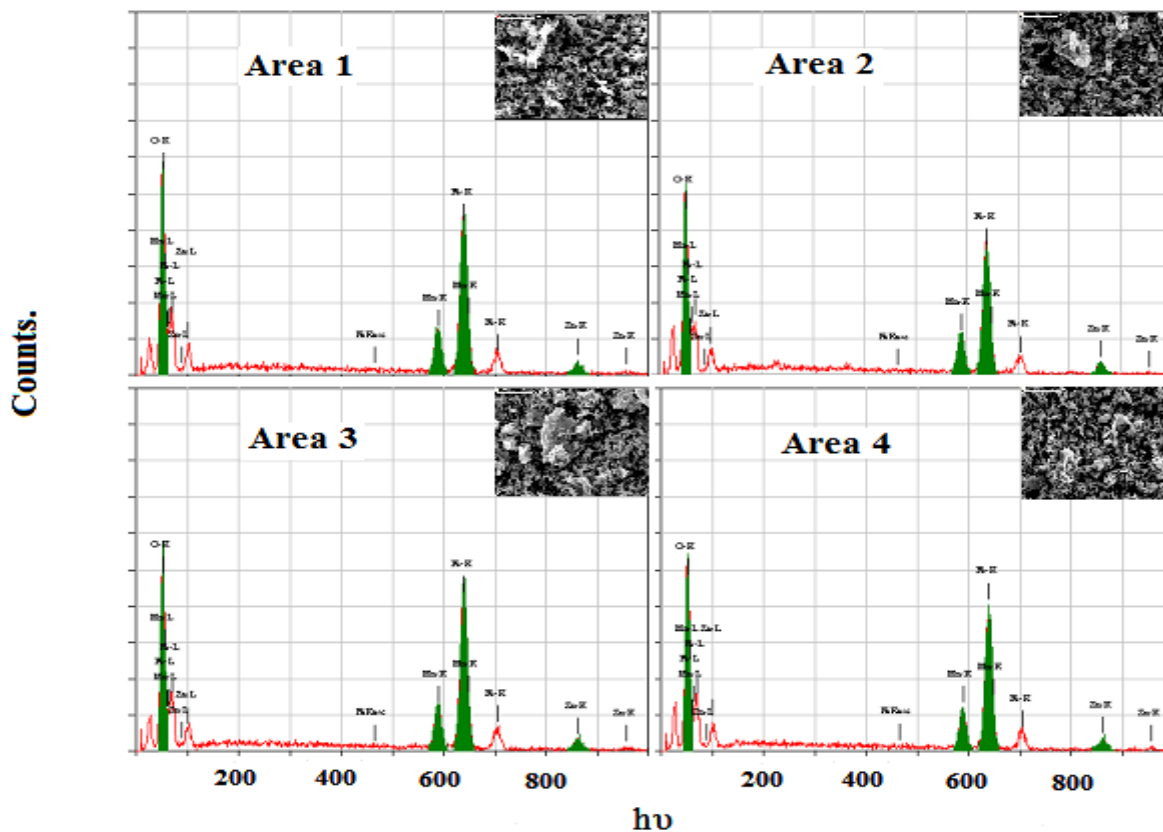


Figure 4. EDX pattern $Mn_{0.5}Zn_{0.5}Fe_2O_4$ sample with different areas.

EDX investigation of the as prepared sample showed the effective atomic concentration of Mn, Zn, Fe and oxygen species at top surface layers of $Mn_{0.5}Zn_{0.5}Fe_2O_4$ sample. The relative atomic abundance of Mn, Zn, Fe and O species present in the uppermost surface and bulk layers of $Mn_{0.5}Zn_{0.5}Fe_2O_4$ sample are given in Tables 1 and 2.

3.3.1. The elements gradient

EDX measurements at 10, 15 and 20 keV showed the concentration of Mn, Zn, Fe and oxygen species from the uppermost surface to the bulk layers. Inspection of Table 1 revealed that: (i) the surface concentrations of Mn species are very close to those in the bulk of the as synthesized specimen. (ii) The surface concentrations of Fe and Zn species are bigger than that in the bulk of sample investigated. (iii) Examination of the uppermost surface layer at 10, 15 and 20 keV resulted in determination of the elements gradient of sample in this layer. In fact, the concentration of Fe species increases as the applied voltage increases from 10 to 20 keV. Opposite behavior was observed in the of Zn species. (iv) The surface concentrations of oxygen species are lower than that in the bulk of sample investigated. These findings suggest a possible redistribution of cations inside the cubic spinel $Mn_{0.5}Zn_{0.5}Fe_2O_4$ powders. So, unique properties of the as prepared sample may be observed depending upon the previous redistribution of cations in the spinel structure.

3.3.2. Homogeneity of the as prepared sample

Tables 1 and 2 showed that the surface concentrations of Mn, Zn, Fe and oxygen species at 20 keV on five different areas over the surface of specimen studied are much closed to each other. This indicates the homogeneous distribution of Mn, Zn, Fe and O species in the investigated sample at 20 keV. Thus, the combustion route is easy to control the stoichiometry and crystallite size which have important influences on structural, morphology, magnetic and electric properties of ferrites.

Table 1. The atomic abundance (surface and bulk) of elements measured at different voltages over the same area for the as prepared solids.

Elements	Atomic abundance (%)			
	Calculated (Bulk)	Found (Surface)		
		10 keV	15 keV	20 keV
O	27.12	19.15	22.50	22.50
Fe	47.41	33.68	54.90	54.89
Zn	13.85	38.07	23.60	23.61
Mn	11.62	09.10	11.28	12.21

Table 2. The atomic abundance (surface) of elements measured at 20 keV and different areas over the as prepared solids.

Elements	Area 1	Area 2	Area 3	Area 4
O	26.73	27.53	24.65	26.55
Fe	53.33	49.66	54.25	51.83
Zn	08.23	10.62	09.05	09.86
Mn	11.71	12.19	12.05	11.76

3.4. Magnetic properties

The saturation magnetization (M_s), remanent magnetization (M_r) and the coercivity (H_c) of the as-prepared powders were determined by measuring the magnetic hysteresis loop (not given) at room temperature. The M_s value was found to be 85emu/g and the value M_r was 22emu/g for the $Mn_{0.5}Zn_{0.5}Fe_2O_4$ sample. The corresponding squareness ratio (M_r/M_s) was found to be 0.259. In addition, the coercivity of the investigated sample was found to 58 Oe. . It was found that the as-prepared $Mn_{0.5}Zn_{0.5}Fe_2O_4$ particles exhibited a saturation magnetization greater than that of $MnFe_2O_4$ and $ZnFe_2O_4$ [14, 16].

4. DISCUSSION

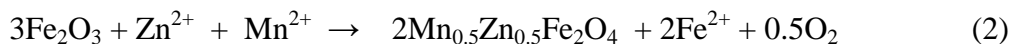
Spinel Mn ferrite, $MnFe_2O_4$, based materials can be prepared via solid state reaction between MnO and Fe_2O_3 [16]. Different factors affect the thermal diffusion of Mn and Fe cations through the early manganese ferrite film which covers the surfaces of grains of reacting oxides (MnO and Fe_2O_3) and acts as energy barrier. These factors are the precursor compounds, preparation method and preparation conditions. In previous our works, we reported that the glycine based combustion route resulted in formation of nano-crystalline zinc and manganese ferrites with a good magnetism [14, 16].

In this investigation, we aim to prepare mixed ferrite with the composition of $Mn_{0.5}Zn_{0.5}Fe_2O_4$ by using modified combustion method. This achieved by using a mixture of glycine and ammonium nitrate. This activation for the combustion method brought about liberation of large amounts from gases with subsequent dissipation for the heat of combustion reaction through the whole mass leading to reduction of local partial sintering among the primary particles. So, ammonium nitrate can be used as promoter for the glycine process for formation of moderate crystalline $Mn_{0.5}Zn_{0.5}Fe_2O_4$ powders. Indeed, using of a mixture of glycine and ammonium nitrate led to reduction in the aggregation process as shown in SEM micrographs.

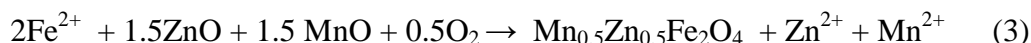
The counter-diffusion of Mn^{2+} , Zn^{2+} and Fe^{3+} through a relatively rigid ferrite film led to the formation of $Mn_{0.5}Zn_{0.5}Fe_2O_4$ particles [14, 16]. Alper reported that the diffusing ions might be Fe^{2+} including Fe^{3+} on the basis of detecting Fe^{2+} in the interface [23]. In addition, following reactions indicate that Fe_2O_3 decomposes to $2Fe^{2+}$ and oxygen gas at Fe_2O_3 -interface [24]. Moreover, oxygen

moves through the reacted area to be added to the ZnO interface and form spinel by reacting with Fe^{2+} , MnO and ZnO:

At Fe_2O_3 interface:



At ZnO and MnO interfaces:



The presence of any Fe^{3+} ions in ZnO and MnO by diffusion would contribute to the chemically created vacancies depending upon the ionic radii of ferric, zinc and manganese species are 0.064, 0.074 and 0.08 nm, respectively [14, 16]. However, 1.5Zn^{2+} and 1.5Mn^{2+} could be replaced by 2Fe^{3+} and a vacancy because of electro-neutrality restrictions. Ferric cations which appear in tetrahedral sites with the introduction of trivalent cations into ZnO or MnO can be considered as an embryonic element or nucleus for formation of inverse spinel in order to satisfy energy stabilization in the structure [25]. On the other hand, Fe^{3+} cations have a tendency to be located in tetrahedral sites with making a strong bond with O^{2-} ions in terms of electro-negativity differences and reach the lowest state of energy [25].

$\text{Mn}_{0.5}\text{Zn}_{0.5}\text{Fe}_2\text{O}_4$ nano-particles prepared by a mixture of glycine and ammonium nitrate has saturation magnetization (85 emu/g) greater than that for Zn ferrite (52 emu/g) and Mn ferrite (67.18 emu/g) due to the redistribution of the reacting cations on A and B sites involved in the spinel Mn-Zn ferrite [14, 16]. In other words, the higher saturation magnetization of $\text{Mn}_{0.5}\text{Zn}_{0.5}\text{Fe}_2\text{O}_4$ prepared in this investigation could be attributed migration of some Fe^{3+} ions from B site to A site with subsequent increase in the $\text{Fe}_A^{3+}\text{-Fe}_B^{3+}$ super-exchange interactions [14, 16].

5. CONCLUSIONS

Formation of the mixed ferrite with composition of $\text{Mn}_{0.5}\text{Zn}_{0.5}\text{Fe}_2\text{O}_4$ via promoted combustion method by using a mixture of glycine and ammonium nitrate has been studied. This method led to formation of $\text{Mn}_{0.5}\text{Zn}_{0.5}\text{Fe}_2\text{O}_4$ with moderate crystalline cubic spinel structure, homogeneously distributed nano-particles and nano-scale size. The as synthesized powders are spongy and fragile. The saturation magnetization (85 emu/g) and coercivity values (58 Oe) of $\text{Mn}_{0.5}\text{Zn}_{0.5}\text{Fe}_2\text{O}_4$ are greater than those for nano-magnetic Zn- or Mn- ferrite materials. This increase in the values of M_s and H_c could be attributed to the redistribution of cations between the tetrahedral and octahedral site involved in the spinel structure. One can not ignore the effect of particle size on the magnetic properties of the as prepared powders.

ACKNOWLEDGEMENT

The project was supported by the Research Center, College of Science, King Saud University.

References

1. Y. Yin, A.P. Alivisatos, *Nature* (London) 437 (2005) 664.
2. M.A. El-Sayed, *Acc. Chem. Res.* 37 (2004) 326.
3. B.Y. Geng, J.Z. Ma, X.W. Liu, Q.B. Du, M.G. Kong, L.D. Zhang, *Appl. Phys. Lett.* 90 (2007) 043120.
4. A.H. Lu, E.L. Salabas, F. SchÜ th, *Angew. Chem.* 46 (2007) 1222.
5. N. M. Deraz, *Ceramics International* 38 (2012) 511.
6. N. M. Deraz, A. Alarifi, *J. Anal. App. Pyrolysis*, 94 (2012) 41.
7. N. M. Deraz, A. Alarifi, *Int. J. Electrochem. Sci.* 7 (2012) 4585.
8. N. M. Deraz, A. Alarifi, *Int. J. Electrochem. Sci.* 7 (2012) 3798.
9. N. M. Deraz, A. Alarifi, *Int. J. Electrochem. Sci.* 7 (2012) 3809.
10. Santosh S. Jadhav, Sagar E. Shirsath, B. G. Toksha, S. M. Patange, S. J. Shukla, K. M. Jadhav, *Inter. J. Mod. Phys. B* 23 (2009) 5629.
11. Jyotsendu Giri, Sriharsha T., Bhadur D., *J. Mater. Chem.* 14 (2004) 875.
12. Simon Thompson, Neil J. Shirtcliffe, Eoins O'Keefe, Steve Appleton, Carole C. Perry, *J. Magn. Mater.* 292 (2005) 100.
13. Jiangno Huang, Hanrui Zhnang, Wen Lan Li, *J. Mater. Res. Bull.* 38 (2003) 149.
14. N. M. Deraz, A. Alarifi, *Polyhedron*, 28(2009) 4122.
15. R. Iyer, R. Desai, R.V. Upadhyay, *Bull. Mater. Sci.* 32 (2009) 141.
16. N. M. Deraz, S. Shaban, , *J. Anal. App. Pyrolysis*, 86 (2009) 173.
17. R. Justin Joseyphus, A. Narayanasamy, K. Shinoda, B. Jeyadevan, K. Tohji, *J. Phys. Chem. Solids* 67(2006)1510.
18. Q. A. Pankhurst, J. Connolly, S. K. Jones, J. Dobson, *Journal of Physics D* 36(2003) R167.
19. R. Jurgons, C. Seliger, A. Hilpert, L. Trahms, S. Odenbach, C. Alexiou, *Journal of Physics: Condensed Matter* 18(2006) S2893.
20. A. C. F. M. Costa, E. Tortella, M. R. Morelli, R. H. G. A. Kiminami, *J. Magn. Mater.* 256(2003)174.
21. A. Verma, T. C. Goel, R. G. Mendiratta, M. I. Alam, *Mater. Sci. Engin.B* 60(1999)156.
22. B.D. Cullity, *Elements of X-ray Diffraction*, Addison-Wesly Publishing Co. Inc. 1976 (Chapter 14).
23. Alper, *High Temperature Oxides*, Academic Press, New York, 1970.
24. A. Azhari, M. Sharif Sh., F. Golestanifard, A. Saberi, *Mater. Chem. Physics* 124 (2010) 658.
25. S.L. Blank, J.A. Pask, *J. Am. Ceram. Soc.* 52 (1969) 669.